12th International Symposium on Turbulence and Shear Flow Phenomena (TSFP12)
Osaka, Japan (Online), July 19–22, 2022

FRACTAL PROPERTIES OF ATOMIZING TURBULENT TWO-PHASE JETS

Josef Hasslberger, Elias Trautner & Markus Klein
Institute of Applied Mathematics and Scientific Computing
Department of Aerospace Engineering, University of the Bundeswehr Munich
Werner-Heisenberg-Weg 39, 85577 Neubiberg, Germany
josef.hasslberger@unibw.de

INTERFACES IN TURBULENT FLOWS

Using a power law ansatz, fractal theory based sub-grid scale modeling is a popular approach in the Large Eddy Simulation (LES) of reactive flows, e.g. combustion. Due to the flame-interface analogy, a similar closure problem exists for interface-dominated multi-phase flows, as further elaborated by Klein *et al.* (2019); Hasslberger *et al.* (2020). The filtered surface tension term in multi-phase LES reads $\overline{\sigma\vec{n}\kappa|\nabla\alpha|}$ (using the surface tension coefficient σ, interface curvature κ, interface normal $\vec{n}=\nabla\alpha/|\nabla\alpha|$, volume fraction α) but cannot be evaluated directly in a-posteriori LES.

According to literature, the flame iso-surface in the flamelet regime (Kerstein, 1988) is characterized by a fractal dimension D_f of $7/3=2.333$, while the maximum for a flame in the well-mixed regime (Hawkes *et al.*, 2012) as well as a passive scalar iso-surface (Mandelbrot, 1975) has been found to be $8/3=2.666$. A theoretical maximum of $D_f=3$ is given by the dimensionality of the confining three-dimensional Euclidean space.

Hence, it is the goal of this study to examine the fractal properties of atomizing multi-phase jets and to indicate a potential modeling strategy for LES of such flows.

DIRECT NUMERICAL SIMULATION DATABASE

The open-source solver PARIS[1] (Aniszewski *et al.*, 2021) is based on the one-fluid formulation of the unsteady incompressible Navier-Stokes equations including capillary forces. Two immiscible fluids are represented by a jump in density and viscosity. Propagation of the phase interface is implicitly calculated by an advection equation for the cell-based volume fraction α of one of the phases. State-of-the-art interface treatment is based on a geometrical Volume-of-Fluid method including piece-wise linear interface reconstruction and a height function method for interface curvature calculation. The code uses a second-order Runge-Kutta technique for time integration and second-order spatial discretization is realized by the finite-volume approach on a regular, cubic staggered grid with a QUICK scheme for momentum advection and central differencing for diffusive fluxes. The projection method invokes a successive over-relaxation solver for the pressure Poisson equation.

In the simulation configuration, the liquid is injected through a round nozzle into an ambient gas and the interface immediately starts to wrinkle according to the turbulent inflow conditions. Interface corrugations grow in downstream direction and ligaments are formed. These ligaments are being stretched, eventually rupture and form droplets. Secondary atomization, i.e. the breakup of droplets into smaller droplets, is naturally included in the simulation but is not at the focus of this work.

The rectangular computational domain extends $12D$ in axial direction and $6D$ in both lateral directions, where D denotes the diameter of the round nozzle. Spatial discretization by a uniform Cartesian mesh of grid size $\Delta=D/64$ yields an overall number of $768\times384\times384\approx1.13\times10^8$ computational cells. At the side boundaries, homogeneous Neumann conditions are imposed, including a narrow band where the velocity is filtered to avoid numerical instabilities. At the outflow boundary, back-flow into the domain is prevented by clipping negative velocities to zero, also for stability reasons. To imitate a turbulent nozzle flow at the inlet, a mean velocity profile is superimposed by a homogeneous isotropic fluctuation level of $u'/U_0=5\%$ and an integral turbulent length scale of $L_t=D/4$ based on the scaling and Gaussian filtering of random fluctuations (Klein *et al.*, 2003). Corresponding to Diesel engine conditions at a pressure of around 5.2 MPa and a temperature of around 900 K, the density and dynamic viscosity ratio are specified as $\rho_l/\rho_g=40$ and $\mu_l/\mu_g=40$, respectively. The liquid viscosity μ_l and the surface tension σ are adjusted according to the inflow-based Reynolds number $\mathrm{Re}=\rho_l U_0 D/\mu_l$ and Weber number $\mathrm{We}=\rho_l U_0^2 D/\sigma$ in Table 1, respectively. The same database has been used earlier to study the flow topology in both phases of atomizing liquid jets (Hasslberger *et al.*, 2019). For one of the cases, i.e. $\mathrm{Re}=5000$ & $\mathrm{We}=5000$, Fig. 1 (top) provides an impression of the topologically complex interface.

Based on the prescribed turbulence quantities at the inlet, relevant length scales characterizing this problem are presented in Table 1: Kolmogorov scale

$$l_K \approx L_t \mathrm{Re}_t^{-3/4} = L_t \left(\frac{u' L_t}{\nu_l}\right)^{-3/4}, \tag{1}$$

Taylor microscale

$$l_T \approx \sqrt{10} L_t \mathrm{Re}_t^{-1/2} \tag{2}$$

and Hinze scale

$$l_H \approx C_H \left(\frac{\sigma}{\rho_l}\right)^{3/5} \varepsilon^{-2/5} \tag{3}$$

[1] http://www.ida.upmc.fr/~zaleski/paris/

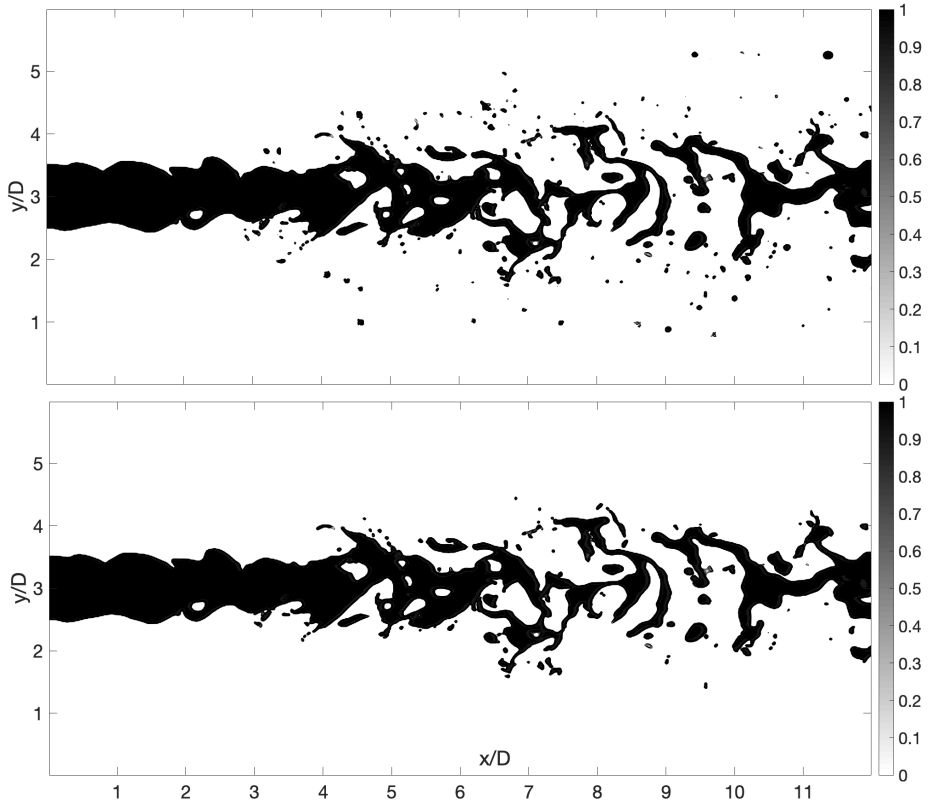

Figure 1. DNS database: Slices of the volume fraction contour for the Re = 5000 & We = 5000 case. Top: core+droplets; bottom: jet core only.

with $C_H = 0.5$ according to Deike *et al.* (2016). The turbulence dissipation is calculated as $\varepsilon = k^{3/2}/L_t = (3/2)^{3/2}(u')^3/L_t$.

Table 1. DNS database: Estimated Kolmogorov scale l_K, Taylor microscale l_T and Hinze scale l_H, all non-dimensionalized by nozzle diameter D, depending on the Reynolds and Weber numbers.

Re-We	l_K/D	l_T/D	l_H/D
2000-2000	0.02236	0.1581	0.0857
2000-5000	0.02236	0.1581	0.0495
5000-2000	0.01125	0.1	0.0857
5000-5000	0.01125	0.1	0.0495

A-PRIORI FRACTAL ANALYSIS

Following fractal theory, the wrinkling of the interface Ξ can be expressed by the power law ansatz

$$\Xi \equiv \frac{\overline{|\nabla\alpha|}}{|\nabla\overline{\alpha}|} = \left(\frac{\eta_o}{\eta_i}\right)^{D_f-2}, \qquad (4)$$

where the outer cut-off scale η_o is given by the filter width Δ in the context of explicit filtering (a-priori analysis). Upon volume averaging, indicated by $\langle\cdot\rangle$, and taking the logarithm, one obtains

$$\log\left(\frac{\langle\overline{|\nabla\alpha|}\rangle}{\langle|\nabla\overline{\alpha}|\rangle}\right) = (D_f-2)\log(\Delta) - (D_f-2)\log(\eta_i), \qquad (5)$$

which can be interpreted as a straight line equation with a slope of $D_f - 2$ in the double-logarithmic diagram. The intersection of the straight line fit with the line given by $\Xi = 1$ yields the inner cut-off scale η_i. In agreement with expectations, Fig. 2 demonstrates that the self-similar fractal behavior can only be observed for large normalized filter widths Δ/D. Accordingly, the linear fit is based on the last few data points in this regime. The procedure is described in more detail by Bambauer *et al.* (2021), for instance.

As summarized in Table 2, the fractal dimension D_f is close to the asymptotic reference value of $8/3 = 2.666$ in two out of four cases. Smaller values of D_f are likely due to insufficient atomization, hence wrinkling of the interface, under the least violent conditions (Re = 2000 & We = 2000). Under the most violent conditions considered here (Re = 5000 & We = 5000), a significant number of disconnected droplets can be observed. In order to isolate the wrinkling of the connected inner core region, a flood fill algorithm is applied to remove the droplets and examine only the jet core in an additional artificial case. A visual comparison of those cases is shown in Fig. 1. Note that thin ligaments can be connected in the third dimension which is not evident from this two-dimensional slice. Now, after removal of separated droplets, the passive scalar reference value of 8/3 is approached in all three cases under sufficiently violent conditions. This is also consistent with the fact that increasing the Weber number decreases the multi-

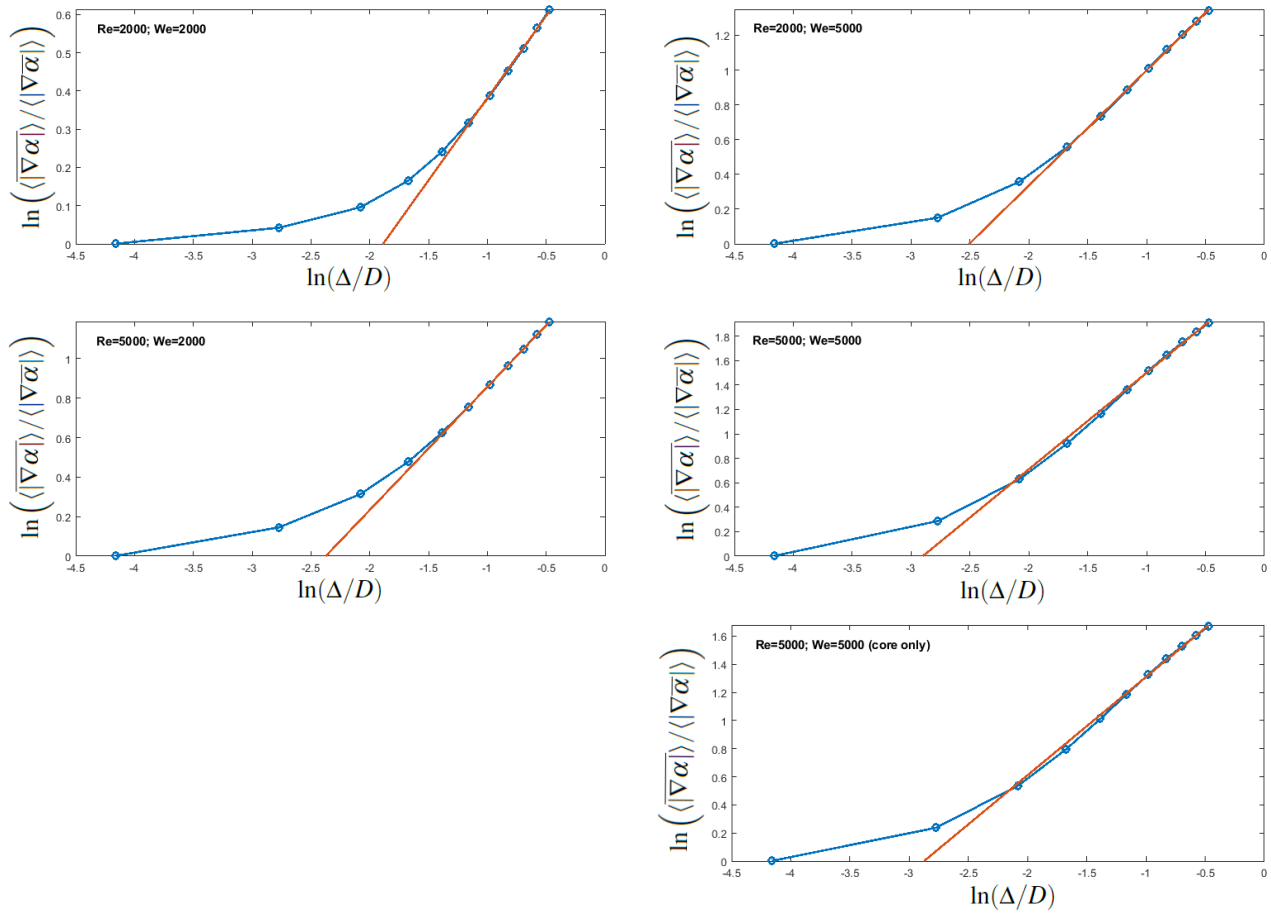

Figure 2. A-priori analysis: Averaged interface wrinkling Ξ depending on the normalized filter width Δ/D for all four Re-We cases. Last row: the Re = 5000 & We = 5000 case with droplets removed (i.e. jet core only). Blue marker symbols: measured values; red line: linear fit in the double-logarithmic diagram. Note the different scales of the ordinate axes.

Table 2. A-priori analysis: Fractal dimension D_f and normalized inner cut-off scale η_i/D, depending on the Reynolds and Weber numbers.

Re-We	D_f	η_i/D
2000-2000	2.4303	0.1515
2000-5000	2.6626	0.0816
5000-2000	2.6238	0.0931
5000-5000	2.7898	0.0550
5000-5000 (core only)	2.6984	0.0564

phase character of the flow with respect to the singular surface tension force at the interface.

Comparing the measured inner cut-off scale η_i in Table 2 with the estimated characteristic length scales in Table 1, it can be stated that the Taylor and Hinze scales are both on the same order as the inner cut-off scale. The fractal behavior might be dominated by the smaller or larger of both. The Kolmogorov scale is about one order of magnitude smaller. In the context of breakup (and coalescence), the Taylor microscale and the Hinze scale are also discussed in the literature (Saeedipour *et al.*, 2016; Ling *et al.*, 2019; Rivière *et al.*, 2021).

A-POSTERIORI LES ANALYSIS

The above analysis suggests a model for the total filtered surface tension term, comprising the resolved and the sub-grid scale contribution, along the lines of

$$\overline{\sigma\vec{n}\kappa|\nabla\alpha|} = \sigma\overline{\vec{n}\kappa}^{s}\,\overline{|\nabla\alpha|} \approx \sigma\overline{\vec{n}}\,\overline{\kappa}|\nabla\overline{\alpha}|\left(\frac{\eta_o}{\eta_i}\right)^{D_f-2} \approx \sigma\overline{\vec{n}}\,\overline{\kappa}|\nabla\overline{\alpha}|\left(\frac{2\Delta}{\eta_i}\right)^{8/3-2}, \quad (6)$$

where surface-weighted filtering is defined as $\overline{\phi}^{s} = \overline{\phi|\nabla\alpha|}/\overline{|\nabla\alpha|}$ and the surface-filtered product $\overline{\vec{n}\kappa}^{s}$ is approximated by the product of the corresponding resolved quantities $\overline{\vec{n}}$ and $\overline{\kappa}$. Hence, the separate sub-grid scale contribution reads

$$\sigma\overline{\vec{n}}\,\overline{\kappa}|\nabla\overline{\alpha}|\left[\left(\frac{2\Delta}{\eta_i}\right)^{8/3-2}-1\right]. \quad (7)$$

For the outer cut-off scale, $\eta_o = 2\Delta$ is selected in accordance with Nyquist's criterion. For the inner cut-off scale, three model variants are tested, namely $\eta_i = l_T^{global}$, $\eta_i = l_H^{global}$ and $\eta_i = l_H^{local}$. While the global calculation of the length scales introduced earlier (Eq. 2 and Eq. 3) is based on the prescribed turbulence characteristics at the inlet, the local calculation of the Hinze scale accounts for local variations of the resolved

and sub-grid scale dissipation, i.e.

$$\begin{aligned}\varepsilon &= \varepsilon^{res} + \varepsilon^{sgs} \\ &= 2\nu\overline{S}_{ij}\overline{S}_{ij} + \tau_{ij}^{sgs}\overline{S}_{ij} \\ &= 2\nu\overline{S}_{ij}\overline{S}_{ij} + 2C_{Smago}^2\Delta^2\sqrt{2\overline{S}_{kl}\overline{S}_{kl}}\,\overline{S}_{ij}\overline{S}_{ij},\end{aligned} \tag{8}$$

where the eddy viscosity model by Smagorinsky (1963) has been assumed.

In this a-posteriori analysis, the density and dynamic viscosity ratio are identical to the DNS database of the a-priori analysis, but the jet Reynolds and Weber numbers are increased to somewhat more challenging conditions of Re = 8000 & We = 5000. The computational domain is a rectangular box extending $16D$ in the axial (x) and $6D$ in the lateral (y, z) directions. An equidistant cubic grid with a resolution of $\Delta = D/128$ is used for the reference DNS, leading to a total of around 1.2×10^9 cells, and a resolution of $\Delta = D/16$ is used for all LES, leading to a total of around 2.4×10^6 cells. Instead of including a nozzle geometry in the computational domain, a mean axial inflow velocity profile

$$\langle u_x \rangle = \frac{U_0}{2} - \frac{U_0}{2} \cdot \tanh\left(\frac{\sqrt{(y-y_c)^2 + (z-z_c)^2} - \frac{D}{2}}{2\theta}\right) \tag{9}$$

is prescribed (Stanley *et al.*, 2002) at the round inlet area with diameter D. Here, (y_c, z_c) denotes the center of the nozzle, and the momentum thickness is set to $\theta = D/20$. This inlet velocity profile is superposed by turbulent fluctuations with an integral turbulent length scale of $L_t = D/8$ and a uniform isotropic fluctuation level of 7.5%. This configuration allows for so-called entrainment, which describes the suction of air into the domain across the lateral boundaries. It is noted that the (sub-grid) behavior of the jet core is of primary interest in the present study since separated droplets, including secondary atomization, are conveniently treated by Lagrangian particles in practical LES. Since it is essential to minimize numerical dissipation in LES, momentum advection has been discretized by central differences and the corresponding closure of sub-grid scale stresses has been achieved by the state-of-the-art eddy viscosity model of Nicoud *et al.* (2011).

The zeroth and first order statistics of the axial velocity field, radial velocity field and volume fraction field are presented in Figs. 3, 4 and 5, respectively. Three axial distances from the nozzle exit are considered, ranging from the near-field ($x/D = 4$) to the far-field ($x/D = 12$), to obtain a complete picture of the model performance. For sufficient distance from the nozzle exit, i.e. $x/D = 8$ and $x/D = 12$, the sub-grid surface tension models lead to an improvement with respect to mean fields and the corresponding fluctuation statistics. The several assumptions in Eq. 6, including also the fractal dimension value of $D_f = 8/3$, seem to be better justified in this region. The situation in the near-field ($x/D = 4$) is less unambiguous. Some of the modeling assumptions (fully developed turbulence, sufficient interface fragmentation) are better justified in the far-field than in the near-field. It is also unclear how well the dominant shear layers close to the nozzle exit can be represented on the LES mesh and what the relative effects of the sub-grid stress and sub-grid surface tension models are. In this a-posteriori configuration, the Taylor microscale model variant shows a weaker influence than the Hinze scale model variant since $l_T^{global}/D = 0.044 > l_H^{global}/D = 0.022$ and this appears consistently in the field statistics. Although both the global and local calculation of the Hinze scale lead to robust and reasonable results for this jet atomization case, it is expected that the local calculation is superior in the general case. The phase inversion benchmark (Estivalezes *et al.*, 2022) might be another interesting test case for the fractal theory based modeling. Finally, it can be stated that the consequences of the model on the flow field can be global, meaning that they are visible in the velocity statistics even at the radial positions where $\langle\alpha\rangle \approx 1$ or $\langle\alpha\rangle \approx 0$ in Fig. 5. Albeit the fractal model acts only at the interface, which is most likely at the radial positions where $\langle\alpha\rangle \approx 0.5$, this behavior is explained by the active nature of the volume fraction field feeding back to the momentum equation via the density and viscosity field as well as the surface tension force. For example, a more compact liquid jet, i.e. less fragmented, yields the non-local effect of decreased jet width as measured by the velocity field.

CONCLUSIONS AND OUTLOOK

Using a DNS database of atomizing two-phase jets, the interface wrinkling and its fractal properties have been analyzed. For sufficient atomization, i.e. sufficiently high Reynolds and Weber numbers, the fractal dimension is very similar to the asymptotic value of 8/3 corresponding to a passive scalar in turbulent flows. The Taylor microscale and Hinze scale appear as potential candidates for the inner cut-off scale.

Preliminary a-posteriori LES analysis revealed that all model candidates based on fractal theory show a non-negligible effect on the statistical behaviour of velocity and volume fraction fields. Both a global and local evaluation of the inner cut-off scale result in stable simulations. Although the first model tests are promising (especially in the far-field of the nozzle where sufficient interface fragmentation occurs), a final assessment is yet to be presented because of the multiple models and numerical aspects influencing the overall simulation result.

Future work will therefore be directed towards the interaction of sub-grid surface tension models with different numerical schemes and other recent sub-grid scale models for the closure of momentum advection (Hasslberger *et al.*, 2021). In addition, it is worthwhile to examine a parameterization or dynamic modeling of the fractal dimension.

ACKNOWLEDGEMENTS

Support by the German Research Foundation (Deutsche Forschungsgemeinschaft - DFG, GS: KL1456/1-3) is gratefully acknowledged.

REFERENCES

Aniszewski, W., Arrufat, T., Crialesi-Esposito, M., Dabiri, S., Fuster, D., Ling, Y., Lu, J., Malan, L., Pal, S., Scardovelli, R. *et al.* 2021 Parallel, robust, interface simulator (PARIS). *Computer Physics Communications* **263**, 107849.

Bambauer, M., Chakraborty, N., Klein, M. & Hasslberger, J. 2021 Vortex dynamics and fractal structures in reactive and nonreactive Richtmyer-Meshkov instability. *Physics of Fluids* **33**, 044114.

Deike, L., Melville, W.K. & Popinet, S. 2016 Air entrainment and bubble statistics in breaking waves. *Journal of Fluid Mechanics* **801**, 91–129.

Estivalezes, J.-L., Aniszewski, W., Auguste, F., Ling, Y., Osmar, L., Caltagirone, J.-P., Chirco, L., Pedrono, A., Popinet,

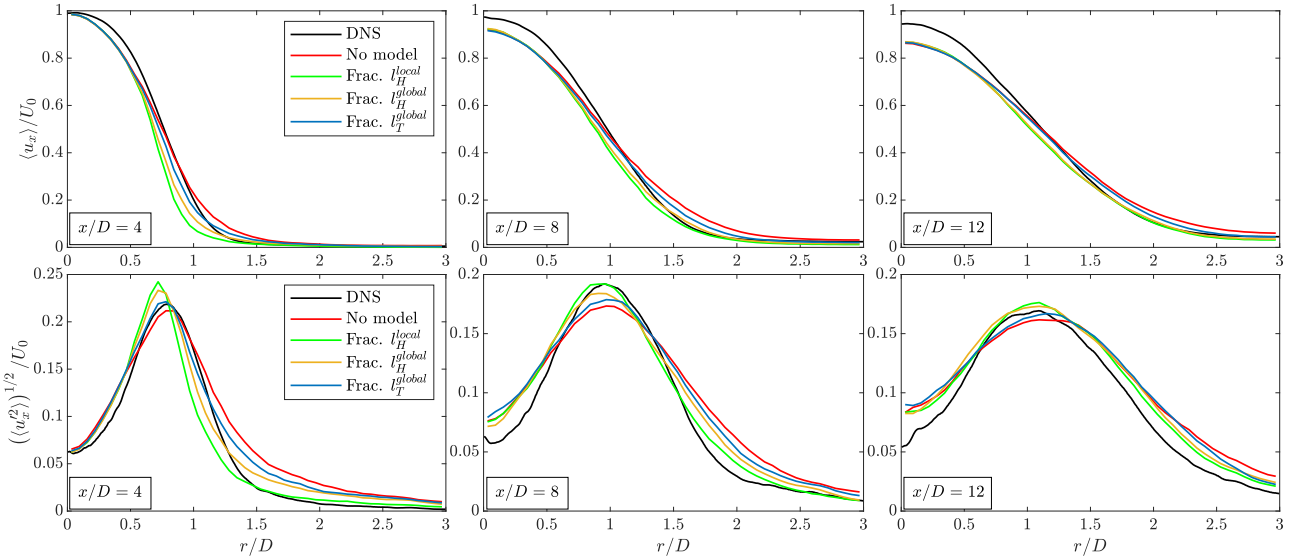

Figure 3. A-posteriori analysis: Radial profiles of the mean axial velocity $\langle u_x \rangle$ and r.m.s. velocity fluctuation $(\langle u_x'^2 \rangle)^{1/2}$ for varying axial distance x/D from the nozzle exit.

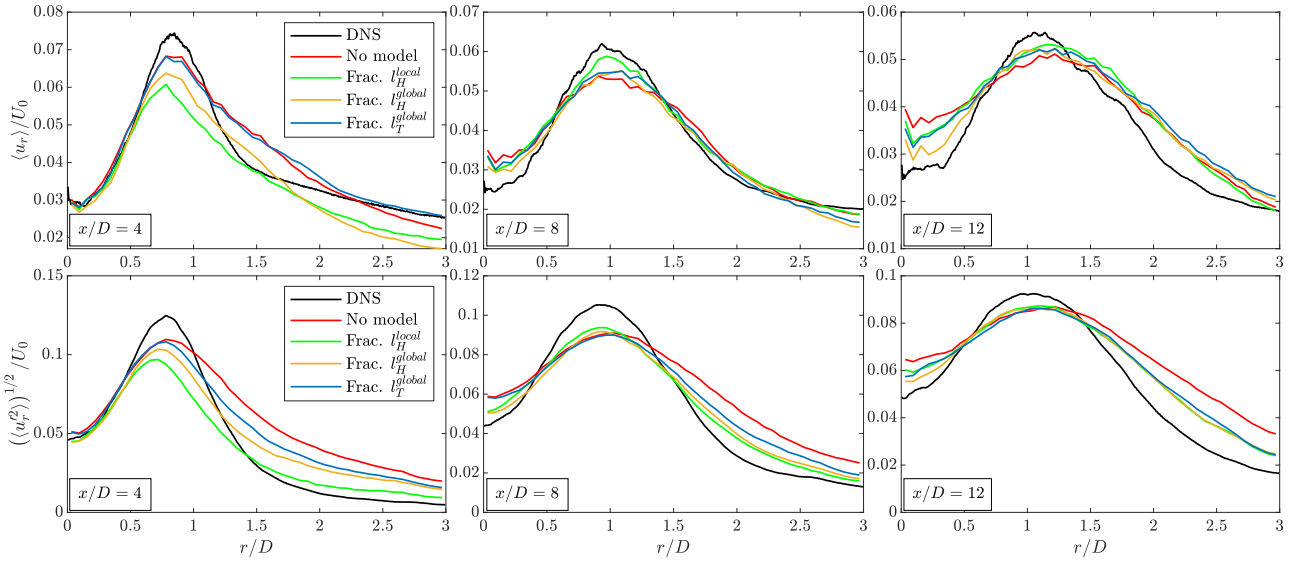

Figure 4. A-posteriori analysis: Radial profiles of the mean radial velocity $\langle u_r \rangle$ and r.m.s. velocity fluctuation $(\langle u_r'^2 \rangle)^{1/2}$ for varying axial distance x/D from the nozzle exit.

S., Berlemont, A. *et al.* 2022 A phase inversion benchmark for multiscale multiphase flows. *Journal of Computational Physics* **450**, 110810.

Hasslberger, J., Engelmann, L., Kempf, A. & Klein, M. 2021 Robust dynamic adaptation of the Smagorinsky model based on a sub-grid activity sensor. *Physics of Fluids* **33** (1), 015117.

Hasslberger, J., Ketterl, S. & Klein, M. 2020 A-priori assessment of interfacial sub-grid scale closures in the two-phase flow LES context. *Flow, Turbulence and Combustion* **105** (2), 359–375.

Hasslberger, J., Ketterl, S., Klein, M. & Chakraborty, N. 2019 Flow topologies in primary atomization of liquid jets: a direct numerical simulation analysis. *Journal of Fluid Mechanics* **859**, 819–838.

Hawkes, E.R., Chatakonda, O., Kolla, H., Kerstein, A.R. & Chen, J.H. 2012 A petascale direct numerical simulation study of the modelling of flame wrinkling for large-eddy simulations in intense turbulence. *Combustion and Flame* **159** (8), 2690–2703.

Kerstein, A.R. 1988 Fractal dimension of turbulent premixed flames. *Combustion Science and Technology* **60** (4-6), 441–445.

Klein, M., Ketterl, S. & Hasslberger, J. 2019 Large eddy simulation of multiphase flows using the volume of fluid method: Part 1 – governing equations and a-priori analysis. *Experimental and Computational Multiphase Flow* **1** (2), 130–144.

Klein, M., Sadiki, A. & Janicka, J. 2003 A digital filter based generation of inflow data for spatially developing direct numerical or large eddy simulations. *Journal of Computational Physics* **186** (2), 652–665.

Ling, Y., Fuster, D., Tryggvason, G. & Zaleski, S. 2019 A two-phase mixing layer between parallel gas and liquid streams: multiphase turbulence statistics and influence of interfacial instability. *Journal of Fluid Mechanics* **859**, 268–307.

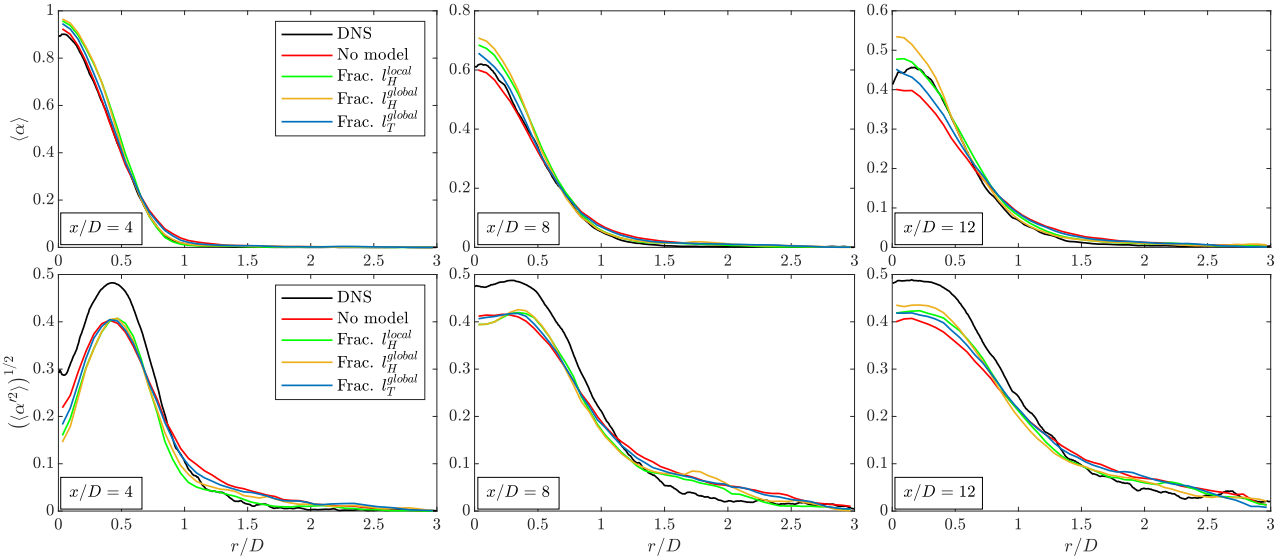

Figure 5. A-posteriori analysis: Radial profiles of the mean volume fraction $\langle\alpha\rangle$ and r.m.s. volume fraction fluctuation $(\langle\alpha'^2\rangle)^{1/2}$ for varying axial distance x/D from the nozzle exit.

Mandelbrot, B.B. 1975 On the geometry of homogeneous turbulence, with stress on the fractal dimension of the iso-surfaces of scalars. *Journal of Fluid Mechanics* **72** (3), 401–416.

Nicoud, F., Toda, H.B., Cabrit, O., Bose, S. & Lee, J. 2011 Using singular values to build a subgrid-scale model for large eddy simulations. *Physics of Fluids* **23** (8), 085106.

Rivière, A., Mostert, W., Perrard, S. & Deike, L. 2021 Sub-hinze scale bubble production in turbulent bubble break-up. *Journal of Fluid Mechanics* **917**.

Saeedipour, M., Pirker, S., Bozorgi, S. & Schneiderbauer, S. 2016 An Eulerian–Lagrangian hybrid model for the coarse-grid simulation of turbulent liquid jet breakup. *International Journal of Multiphase Flow* **82**, 17–26.

Smagorinsky, J. 1963 General circulation experiments with the primitive equations: I. the basic experiment. *Monthly Weather Review* **91** (3), 99–164.

Stanley, S.A., Sarkar, S. & Mellado, J.P. 2002 A study of the flow-field evolution and mixing in a planar turbulent jet using direct numerical simulation. *Journal of Fluid Mechanics* **450**, 377–407.